Open Access
ChemistryOPEN
Full Papers

Structure Formation in Class I and Class II Hydrophobins at the Air–Water Interface under Multiple Compression/Expansion Cycles

Martin Kordts, Melanie Kampe, Andreas Kerth, and Dariush Hinderberger*[a]

Hydrophobins are small amphiphilic fungal proteins empirically divided into two classes. We investigated the self-assembled structures of class I SC3 from *S. commune* and class II HFBII from *T. reesei* transferred to mica from the air–water interface by using the Langmuir–Schaefer (LS) technique and atomic force microscopy (AFM). The main focus is the influence of areal constraint and multiple compressions and expansions on the morphology of the protein films. SC3 shows a rather homogenous coverage of the mica surface, with fibrillary structures. Multiple compressions to a surface pressure of 13 mN m^{-1} led to a shortening of the fibrils. HFBII exhibits multilayered structures of varying thickness at higher surface pressures. Multiple compressions led to a variety of large, multilayer aggregates. Several compressions and expansions homogenized the films of both types. Both proteins showed similar dendritic structures with relevant length scales of at least several hundred nanometers at pressures of 13 mN m^{-1} and above, although the primary structures they assemble into are usually different in size and type, and range from fibrils to hexagonally ordered films. These dendritic structures may stem from a combination of mechanical influences, such as compressions, expansions, and the drying effect during LS transfer, which may simulate processes during physiological applications of hydrophobins, such as encapsulation or release of spores.

1. Introduction

Hydrophobins are small ($\approx$ 7–10 kDa) amphiphilic proteins that originate from filamentous fungi. The primary structure is characterized by a conserved pattern of eight cysteine residues that form four intramolecular disulfide bridges. Early hydrophobin research led to their empirical classification into two classes, namely class I and class II.[1] This classification is based on the solubility of the aggregates they form. Based on the limited biochemical data available at that time, Wessels predicted that class I aggregates would only dissolve in strong acids, such as trifluoroacetic acid (TFA), whereas class II aggregates could dissolve in aqueous dilutions of organic solvents.[2] Although this prediction has been remarkably accurate so far, the biological significance remains largely unclear.

Although both classes initially form similar surface membranes, films of class I hydrophobins transition into insoluble rodlets, whereas class II hydrophobins can dissociate reversibly.[3]

Hydrophobins fulfill multiple roles in fungal development, all of which are attributed to their high surface activity. They are, for example, involved in the infection of host organisms,[4] the prevention of waterlogging,[5] and the formation of protective layers during fruiting body development.[6]

Self-assembled films at the air–water interface lower the surface tension to allow the growth of aerial hyphae. They also coat spores and hyphae to facilitate distribution by wind and attachment of the fungus to solid surfaces, respectively.[7] Within this context, hydrophobins have also been linked to the pathogenicity of numerous fungal species.[8]

Class I rodlets share many structural similarities with amyloid fibrils. They are unbranching, straight, and rich in β-sheet structures. It has been shown that the amount of β-sheet content further increases upon self-assembly at the air–water interface.[2, 9, 10]

Hydrophobins are frequently discussed as emulsifiers, coating agents, and carriers, and in other roles in a plethora of fields, such as biotechnology and the cosmetics industry.[11] Although the self-assembled films and structures of several hydrophobins of both classes have been studied quite extensively in recent years, the influence of external constraints usually gets little attention. It is known, however, that results strongly depend on sample preparation.

Most notably, Yu et al. reported different morphologies of Langmuir–Blodgett (LB) and Langmuir–Schaefer (LS) films when class I hydrophobin HGFI was compressed once or multiple times on a Langmuir trough.[12] Interestingly, their findings differ considerably from the results presented here because

[a] M. Kordts, M. Kampe, Dr. A. Kerth, Prof. Dr. D. Hinderberger
Institut für Chemie, Martin-Luther-Universität Halle-Wittenberg
Von-Danckelmann-Platz 4, 06120 Halle/Saale (Germany)
E-mail: dariush.hinderberger@chemie.uni-halle.de

they found no rodlets at all after a single compression, but very long rodlets after the film was compressed multiple times. This highlights the importance of sample preparation (e.g., substrate, transfer method, deposition pressure) and clearly shows that various class I hydrophobins can appear very different.

Herein we created self-assembled structures at an air–water interface under very specific surface pressures and easily reproduced processing conditions, in particular multiple compression/expansion cycles. After LS transfer to mica surfaces, the formed structures were studied by using atomic force microscopy (AFM) and a remarkable wealth of, for example, large-scale dendritic structures were observed; the underlying processes that lead to the individual structures of both hydrophobin classes are discussed.

2. Results and Discussion

Compression isotherms of both proteins are shown in Figure 1. The initial surface pressure of HFBII after spreading ranged from 1 to 6 mN m^{-1}, and did not reach zero even after stabilization for 18 h. Neither isotherm shows clear indications of a
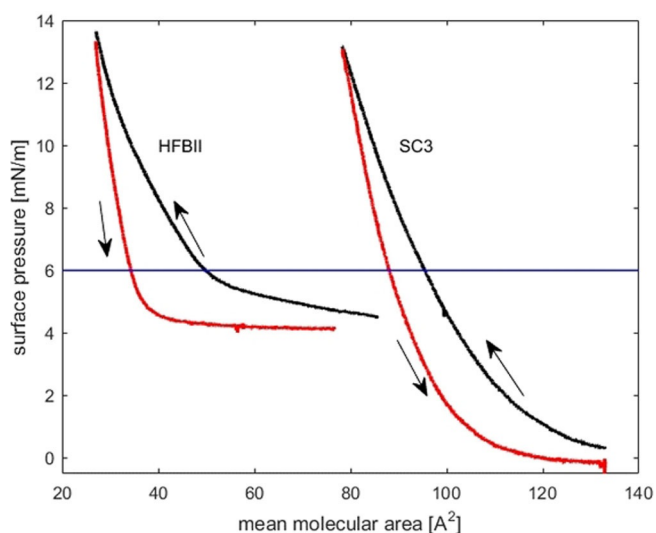

Figure 1. Compression isotherms of SC3 and HFBII.

phase transition (plateau-like behavior) or ripping of the film at higher surface pressures. There is a strong hysteresis between the compression and expansion isotherms. To examine this effect, both proteins were compressed to a surface pressure of 13 mN m^{-1} and then expanded, and the observed areas per molecule at 6 mN m^{-1} were compared. Experience has shown that the maximum error of area values obtained in this way is of the order of $\pm 2\%$. Monomers of SC3 have a diameter of 32 Å,[13] whereas HFBII monomers have dimensions of $24 \times 27 \times 30$ Å, that is, an average diameter of 27 Å.[14] A hierarchy has been proposed for HFBII, which first assembles into tetramers for which the largest diameter is 65 Å.[15] In both cases the area requirement upon expansion is lower than for the compression. This effect is much stronger in HFBII, in both absolute

and relative terms; it displays a difference in molecular area of 15.6 Å^2, compared with 7.45 Å^2 for SC3 (see Table 1). This suggests that both proteins form stable multilayered aggregates that do not disassemble upon expansion. Additional cycles

Table 1. Mean molecular areas [Å^2] and hysteresis at 6 mN m^{-1} between compression and expansion after the second cycle for both hydrophobins.

Sample	Compression	Expansion	Difference
SC3	95.45	88.00	7.45
HFBII	49.91	34.28	15.64

showed no difference compared with the second one, which is in agreement with the findings of Paananen et al., who deduced that no molecules are expelled from the monolayer and thus lost to the subphase during compressions (see Figure 2).[15]
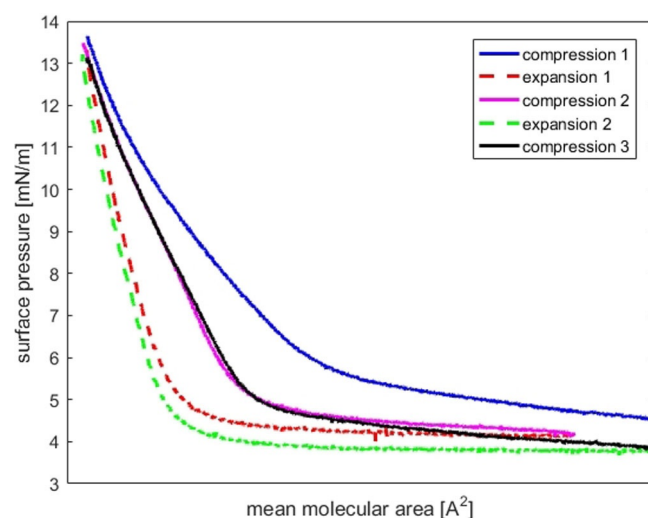

Figure 2. Hysteresis between the compression and expansion isotherms of HFBII. Additional cycles did not differ from the second one.

To compare both proteins by using AFM, samples were transferred to mica at 6.5, 13, 19, and 27.5 mN m^{-1} after one, two, and three compressions and expansions, respectively. Additionally, SC3 was compressed to 1.5 mN m^{-1} and HFBII to 3.3 mN m^{-1} to investigate the initial conditions under weak constraints.

2.1. Single Compression

In the AFM micrographs, SC3 shows a heterogeneous morphology when transferred from the air–water interface at low surface pressures of 1.5 and 6.5 mN m^{-1}. As can be seen in Figure 3A and B, globular aggregates ranging in size from 100 to around 500 nm and fibrils of various length are randomly distributed across the mica surface. In other samples (see Figure SI 1 in the Supporting Information), larger clusters of protein matter with a height of about 25 nm were visible along-
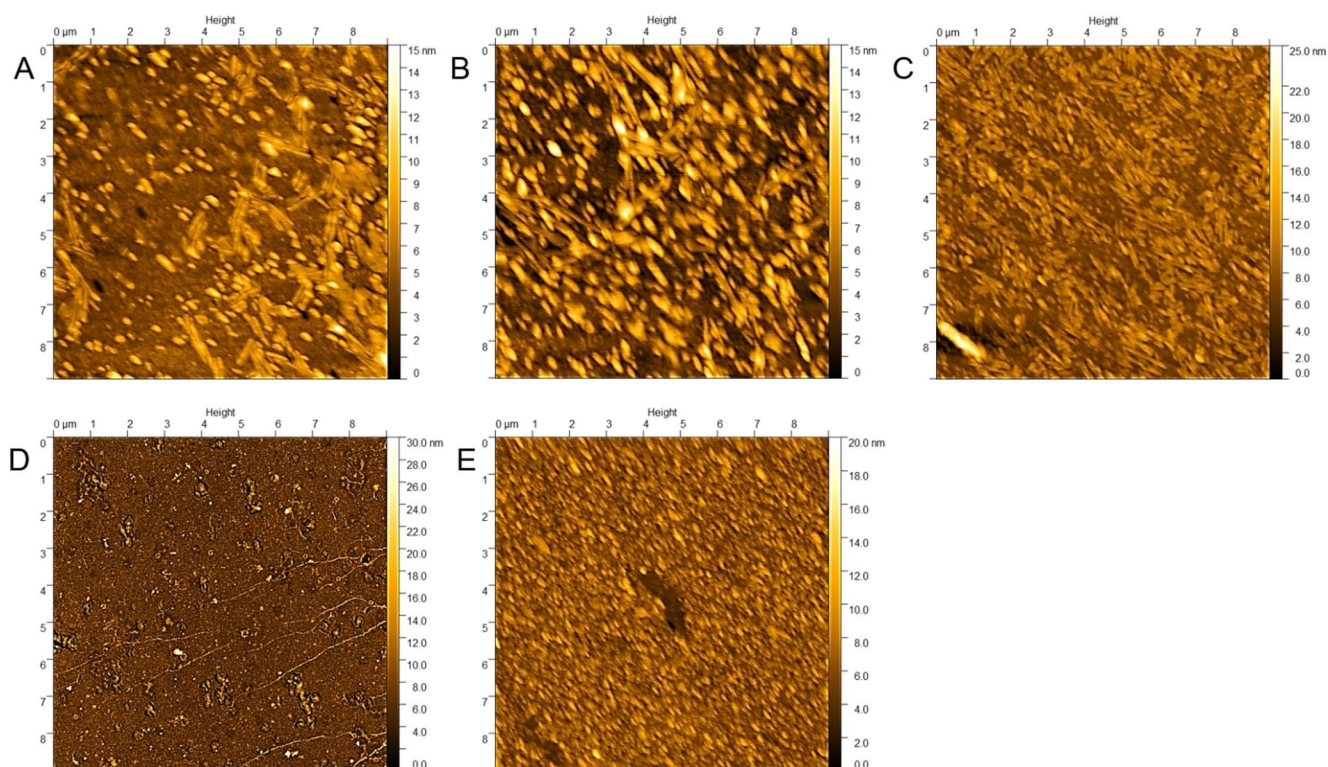
Figure 3. AFM height micrographs of SC3 at different transfer surface pressures: A) 1.5, B) 6.5, C) 13, D) 19, and E) 27.5 mN m^{-1}; dimensions are 9×9 μm^2. For cross-sections, see Addendum 1 in the Supporting Information.

side the clean mica surface. However, because this morphology was observed only in one sample, it is likely a compression artefact. Nonetheless, it indicates the heterogeneity of self-assembled structures without any areal constraint.

With increasing surface pressure, the fibrillary structures dominated and the film became more homogenous (Figure 3C–E). Mica surface coverage rose from about 60% at 1.5 mN m^{-1} to roughly 90% between 6.5 and 27.5 mN m^{-1}, after which it remained relatively stable (see Figure SI 2).

The height distribution derived from the micrographs is displayed in Figure 4. Cross-sections of all micrographs and relevant parameters of the Gaussian fits can be found in the Supporting Information. The lengths and apparent width of these fibrils vary greatly with no clearly visible trend, but the height distribution of the observed structures changes from a bimodal distribution of 2.5 up to 10 nm at low and intermediate pressures (1.5, 6.5, and 13 mN m^{-1}) to a more homogenous distribution centered around 5–6 nm at 27.5 mN m^{-1}.

Although we refrain from interpreting the absolute numbers of both distribution density and height, it is apparent that an initially bimodal distribution (transfer at 1.5–13 mN m^{-1}) becomes very broad (full width at half maximum (FWHM) ≈ 5 nm) and appears monomodal and centered at approximately 11 nm when transferred at a pressure of 19 mN m^{-1}. When the sample was transferred from an even higher pressure of 27.5 mN m^{-1}, the distribution appeared more homogenous, centered at around 7 nm with a FWHM of about 3 nm.

HFBII, on the other hand, shows a rather homogenous film when transferred at a low surface pressure, with a height of roughly 2 nm as shown in Figure 5A, B. Kisko et al. reported a
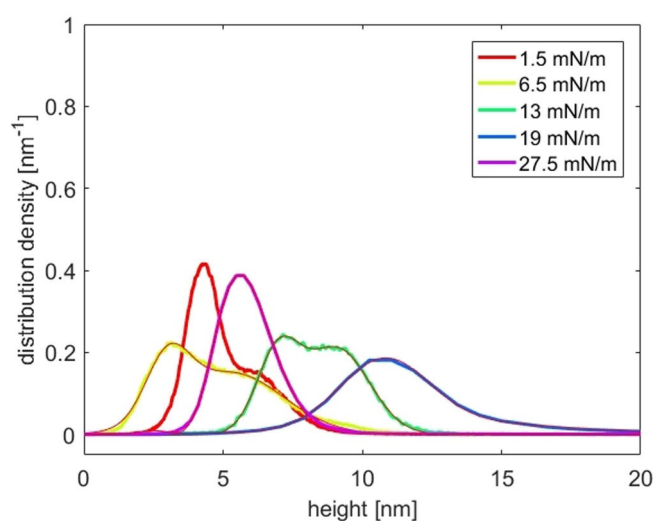

Figure 4. Height distribution of SC3 structures at different surface pressures, as shown in Figure 3; dots represent Gaussian fit.

thickness of about 64 Å for Langmuir–Blodgett films of HFBII transferred at a lateral pressure of 30 mN m^{-1},[16] whereas they found that the protein layer at the air–water interface had a thickness of between 24 and 28 Å.[17] This shows the great importance of sample preparation and the chosen technique and again we refrain from interpreting absolute numbers.

Figure 5 shows height images of HFBII films transferred from the Langmuir trough at different surface pressures. At 3.3 and 6.5 mN m^{-1}, a homogenous protein layer can be seen, on top of which irregular structures with heights of between 4 and
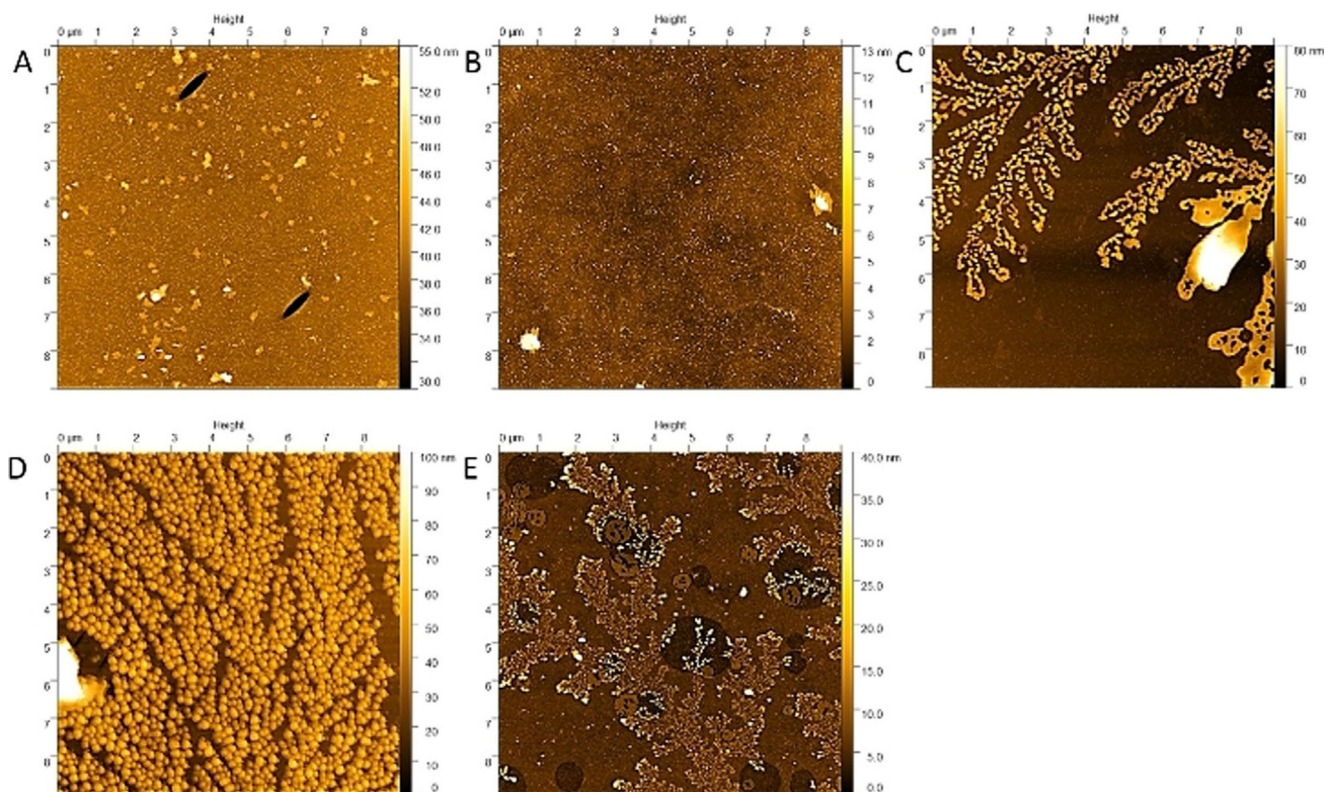
Figure 5. AFM height micrographs of HFBII at different surface pressures: A) 3.3, B) 6.5, C) 13, D) 19, and E) 27.5 mN m^{-1}; dimensions are 9×9 µm^2. For cross-sections, see Addendum 2 in the Supporting Information.

15 nm are present. As the surface pressure before transfer was increased, multilayered structures of varying thickness were formed. Most notably, dendritic structures with heights of between 40 and 100 nm appeared at 13 mN m^{-1} and were still present at higher pressures.

At 19 mN m^{-1}, similar structures 30 nm in height and with a diameter of around 200 nm dominated and were still present at 25 mN m^{-1}, but with decreased height. Figure 6 summarizes the height distribution of HFBII as a function of surface pressure.
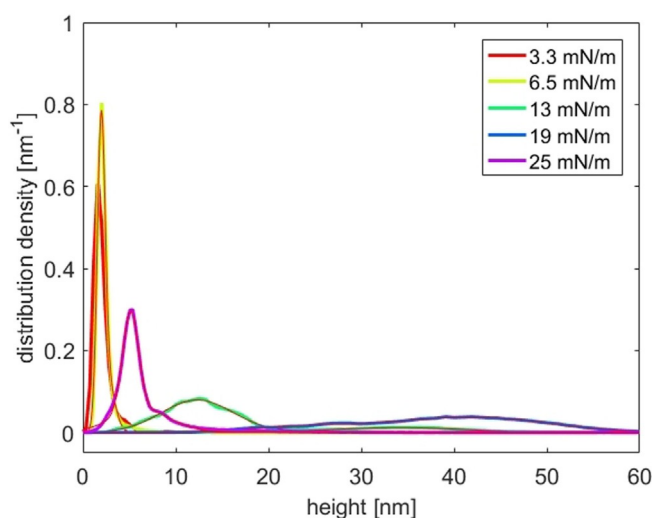

Figure 6. Height distribution of HFBII structures transferred at different surface pressures.

sure. Starting at 2 nm at low pressures, the distribution broadens and the maximum shifts to much larger values of up to 42 nm at 19 mN m^{-1}, then stabilizes at around 5 nm at 25 mN m^{-1}. This steep drop in height at a high lateral pressure may well be an artefact of sample preparation because the film is ripped from the air–water interface and subsequent drying of the sample subjects the transferred film to capillary forces (see also discussion below). Upon reaching a surface pressure of 13 mN m^{-1}, the height distribution shifted from 2 to around 10 nm, large dendritic structures emerged, and the coverage of the substrate increased from approximately 70 to 92 % (see Figure SI 3). A comparison of all height profiles can be found in Addendum 4 in the Supporting Information.

2.2. Multiple Compression/Expansion Cycles

When compressed to 1.5 mN m^{-1} several times before being transferred to mica, SC3 exhibited large spherical aggregates of 100 to 500 nm in diameter along with fibrils that shortened from several hundred nanometers long to around 70 nm and remained present when the film was expanded to zero surface pressure (see Figure SI 4). As can be seen in Figure 7, the height distribution shifts from a bimodal curve with maxima at 4.5 and about 6 nm to a more uniform distribution centered around 2.5 nm. The existing aggregates partially dissolve upon expansion and appear to self-assemble into larger structures. Therefore, the coverage of the mica surface decreases from around 60 to 35 % after three cycles (see Figure SI 5). There is great variation between the images because of this clustering.
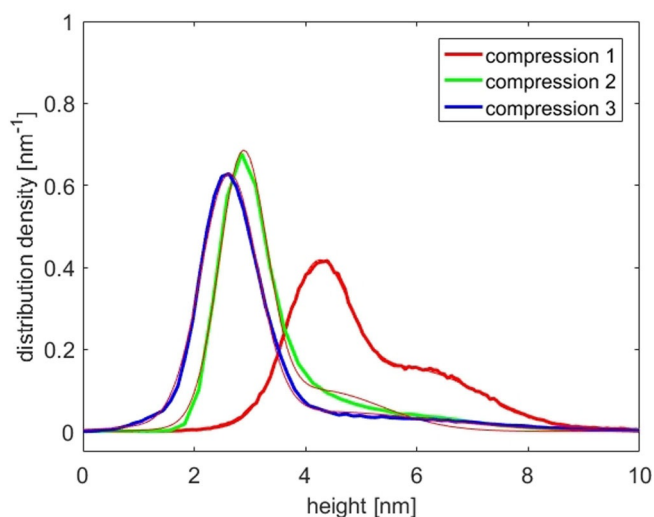
Figure 7. Height distribution of SC3 structures transferred at 1.5 m$_N$ m^{-1} after each compression.

Due to the initial surface pressures of 1 to 6 m$_N$ m^{-1} in the Langmuir trough several hours after injection, HFBII could not be investigated at the low surface pressure of 1.5 m$_N$ m^{-1} used for SC3.

When SC3 was repeatedly compressed to a pressure of 13 m$_N$ m^{-1} (and expanded to low pressure; see Figure SI 6), the fibrillary structures observed after transfer to the AFM shortened drastically from an average length of about 570 nm after the first compression to just over 100 nm after the fourth (see Figure 8A). The apparent width of the fibrils also decreased slightly. This indicates a partial breakdown of the aggregates upon expansion and a preference for the formation of new fibrils over extension of existing ones when the film is compressed again (see Figure 8A). It should be noted that no fibrillary structures could be observed after two compressions.

Although the height distribution shows no clear trend over several compressions, it is clear that the film became more homogenous, as indicated by the shift from a bimodal distribution after the first compression to unimodal curves after each subsequent compression step (see Figure 8B).

The curves for the first and second expansion in Figure 8B show a shoulder that ranges from 2.5 to around 8 nm and coincides with the maxima of preceding compressions. This again suggests that the film does not disintegrate uniformly, but instead larger aggregates remain stable. Samples taken after the film was expanded, however, show a strong broadening of the height distribution curves and a shift in the maxima from 1 to 2 nm after one and two expansions, respectively, to more than 50 nm after the third (see Figure SI 7). As can be seen in Figure SI 6F, this broadening stems from the formation of globular aggregates of varying heights.

In contrast to multiple cycles to a pressure of 1.5 m$_N$ m^{-1}, however, coverage of the mica surface slightly increased and stabilized at around 90 % after several compressions (see Figure SI 8).

HFBII also showed a strong heterogeneity of structures over several compressions to 13 m$_N$ m^{-1} before transfer. As men-
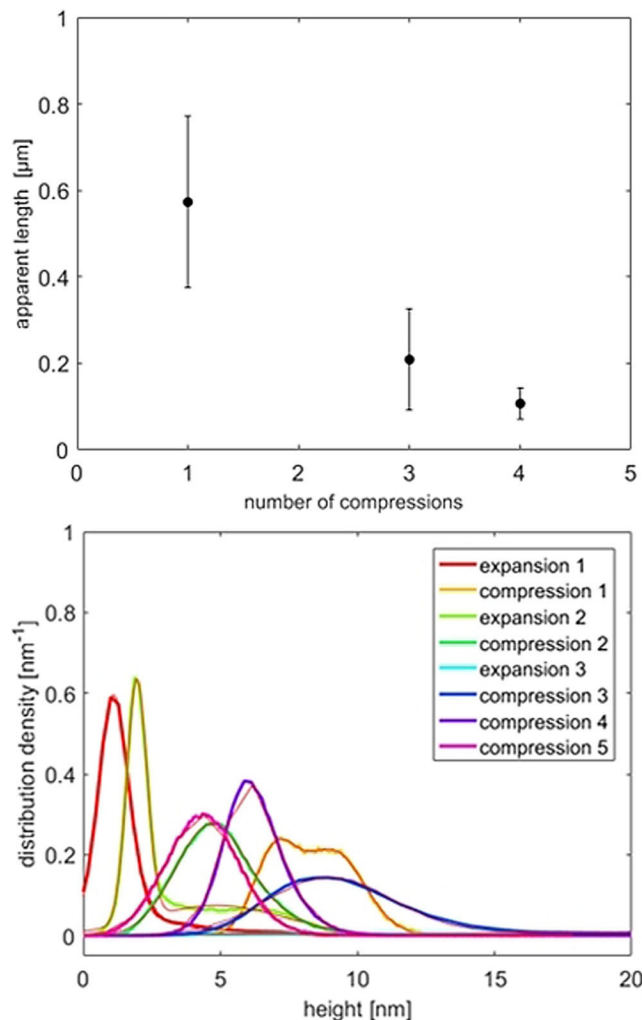

Figure 8. A) Apparent length of SC3 fibers after several compressions and transfer at 13 m$_N$ m^{-1}. B) Height distribution of SC3 aggregates over several compression/expansion cycles to 13 m$_N$ m^{-1}.

tioned above, large dendritic structures with a height of 45 nm were present on top of a dense, closed protein layer after the first compression (Figure 9). These larger structures partly dissolved when the film expanded. In contrast to the class I hydrophobin, however, a closed layer of protein remained stable underneath these larger structures. After the second compression, these larger structures disappeared but the film appeared rather inhomogeneous, with small aggregates randomly distributed on top of the closed layer and several round holes in the top layer. After the third compression, several larger structures with diameters of 40 to between 200 and 300 nm were present. Their height is in the range of 10 to 12 nm. These clusters once again mostly dissolved when the film was expanded.

Figure 10 shows the height distribution of the observed structures for up to three compressions of HFBII to a surface pressure of 13 m$_N$ m^{-1} and subsequent expansions. All compression curves are rather unimodal and the maximum shifted from about 10 to 13 nm after the first compression to about 4 nm after the third compression. The first expansion created a
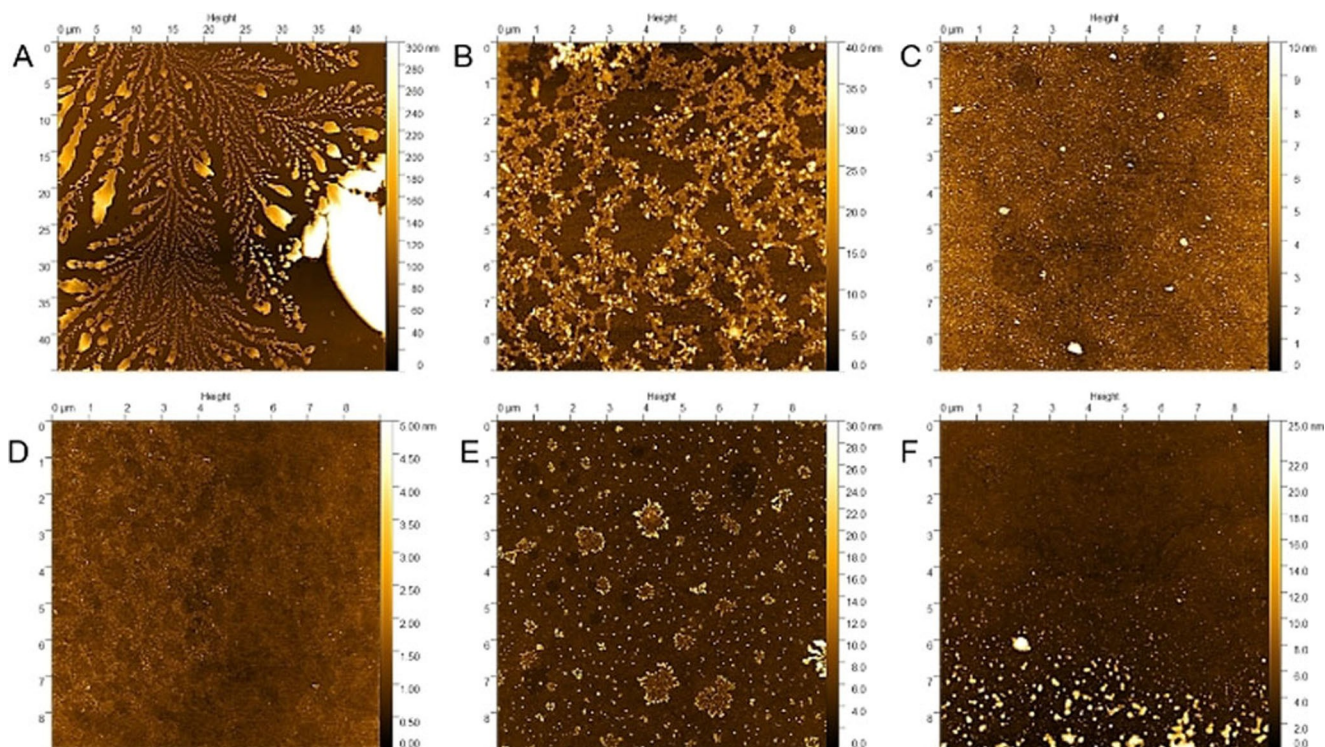
1009

Figure 9. AFM micrographs of HFBII transferred at 13 mN m^{-1}: A) 1 compression, B) 1 expansion, C) 2 compressions, D) 2 expansions, E) 3 compressions, and F) 3 expansions; dimensions are 9×9 µm^2. For cross-sections, see Addendum 3 in the Supporting Information.
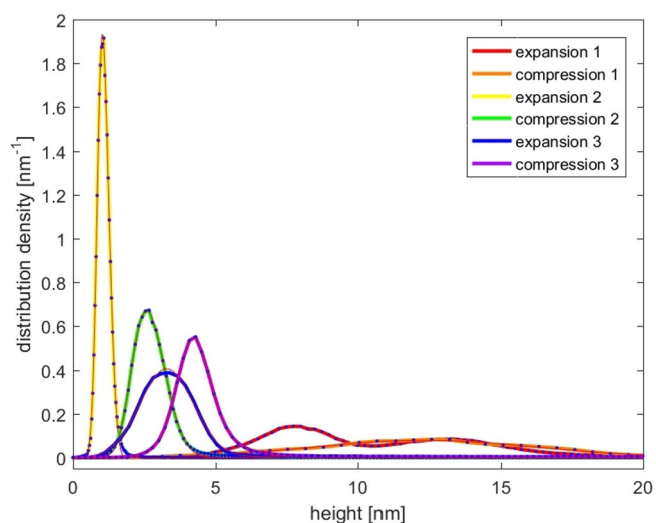

Figure 10. Height distribution of HFBII structures transferred after several compressions to 13 mN m^{-1} and subsequent expansions.

bimodal distribution with maxima of about 7.7 and 13 nm; the latter coincides with the first compression maximum, which again shows the nonuniform dissolution of the film. Coverage of the mica surface ranged from 70 to about 95% and did not change significantly over several cycles. It also tended to be slightly lower for the corresponding expansions, which again supports the observation that the structures dissolve in a nonuniform manner (see Figure SI 9).

The dendritic structures observed after a single compression that, as discussed earlier, are also visible at higher pressures, did not appear if the film was compressed and expanded multiple times. Somewhat similar structures can also occasionally be found in SC3 samples. For comparison, Figure 11B shows an image of SC3 after three compressions and subsequent LS
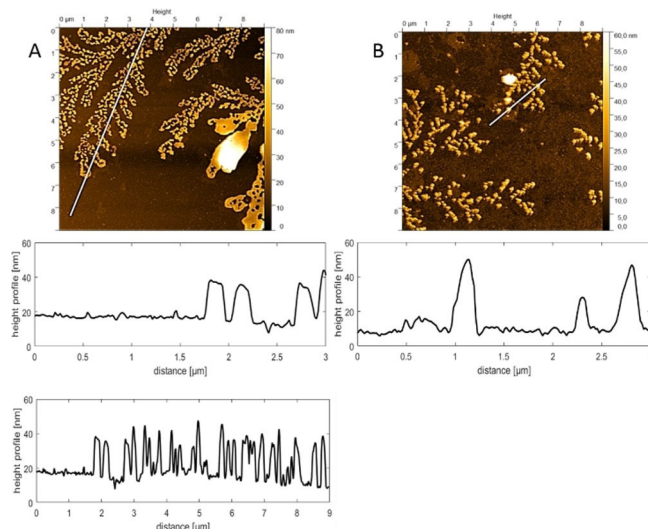

Figure 11. Top: AFM micrographs of A) HFBII and B) SC3 transferred at 13 mN m^{-1} after one and three compressions, respectively; dimensions are 9×9 µm^2. Middle: cross-sections along the white lines, measured in direction of increasing x value. Bottom: Cross-section of HFBII micrograph along the entire white line.

transfer. Although these structures seem more densely packed for HFBII (Figure 11A) and occur more frequently, they are of similar height and size in both proteins. In Figure 11A, a closed protein layer can be seen underneath the dendrites, whereas for SC3, once again, the film is more inhomogeneous and fibrillary structures predominate (Figure 11B).

Given the multitude of constraints at play, it is difficult to explain this phenomenon in a straightforward manner. In AFM studies of hydrophobins, similar dendritic structures have not yet been observed, although monolayers of several members of both class I and class II hydrophobins have been studied quite extensively.

On scrutinizing the literature, however, it becomes apparent that in these earlier studies the surface pressure at the air–water interface is often well adjusted. In addition, to the best of our knowledge, this study is the first report of controlled, multiple compression/expansion cycles on self-assembled monolayers of SC3 and HFBII. Considering the size and heterogeneity still present in the samples in our study, it may well be that in earlier AFM studies large dendritic structures have simply not been seen due to the much higher resolution achieved therein. Furthermore, most studies are performed on small droplets dried on the substrate, or Langmuir–Blodgett (LB) films often transferred to highly oriented pyrolytic graphite (HOPG), for which the dominant interactions between substrate and protein are fundamentally different.[18] Branched structures have been observed for multilayered polymer solutions and were attributed to nonuniform evaporation of the solvent.[19]

Although the system described herein fundamentally differs from those described in Ref. [19], the underlying physics are likely similar. Although the substrate is submersed in water prior to LB transfer and the hydrophobic surface is only partially wetted by ambient water vapor, LS films consist of a complex multiphase system of mica exposed to ambient water vapor, the hydrophobic side, and the strongly wetted hydrophilic side of the protein film. As Karthaus et al. note, at the edges of droplets, that is, in multiphase regions, the Marangoni effect leads to fingering instability and the formation of ordered micron-sized branched structures.[20] The crucial step may be that, during drying on the mica surface, capillary forces due to inhomogeneous evaporation distort the films by changing the dominant interactions from protein–water to protein–protein and protein–air and, therefore, create local inhomogeneities of interfacial tension that lead to the aforementioned effect.

Although the exact mechanics are outside the scope of this study, it is worth noting that similar structures can be observed here for two proteins with vastly different primary aggregates. For HFBII, this morphology is in fact dominant in samples transferred at 13 mN m^{-1} and above. One may then speculate that despite the empirical separation into two classes, the intermolecular interactions behind fibrillation (class I, SC3) and film formation (class II, HFBII) can be fine tuned by external constraints, such as precisely tuned surface pressure, potentially in combination with drying capillary forces, to achieve similar final dendritic structures. Given that drying and surface-

transfer processes are abundant in the natural use of hydrophobins by fungi (e.g., encapsulation or release of spores), the phenomenon characterized herein could lead to a more unified view of hydrophobins, their self-assembled structures, and potentially their natural and artificial uses.

Whether one can design the external constraints in such a manner to obtain specific, more complex structures that differ from the initial fibrillary and two-dimensional structures remains to be seen in future studies.

3. Conclusions

We have shown that multiple compression and expansion cycles have a major influence on the morphology of interfacial structures for class I and class II hydrophobins. Class I SC3 is known to form fibrillary aggregates of different lengths, whereas class II HFBII assembles into a more uniform, multilayered film. For both proteins, the interfacial films tend to become more homogenous when compressed and expanded several times. Neither of the protein films dissolved uniformly upon expansion; rather large clusters of densely packed material remained beside void areas without protein coverage.

Although there is no clear trend in the height distribution for SC3, the fibrils shortened drastically over multiple compressions. The coverage of the substrate surface stabilized at close to 100 % when the film was compressed to a surface pressure of 13 mN m^{-1}. HFBII shows dendritic morphology when transferred to mica at surface pressures of 13 mN m^{-1} and above. These large structures, which may have heights of more than 40 nm, dissolved when the film was compressed multiple times.

Hydrophobins could offer a great variety of options for surface modification and nanostructured functional surfaces. We show that sample preparation, that is, the number of compressions, lateral pressure at transfer, and even the mode of transfer, has a great influence on the surface morphology on a micrometer scale. Interestingly, similar structures were found for both proteins depending on their compression state.

Figure 12 shows a schematic representation of the emergence of large dendritic aggregates that appear to be comprised of globular substructures in both proteins. Although these effectively vanish after several compression/expansion cycles for class II hydrophobin HFBII, they constitute the dominant microscopic morphology in this protein for single compressions to 13 mN m^{-1} and higher. In class I SC3, conversely, dendritic structures emerged only after several steps of constraint and relief.

We argue that these dendritic morphologies are a consequence of the multitude of constraints at play, such as areal confinement and capillary forces during drying of a transferred film, which lead to similar structures at a micrometer scale despite different molecular mechanisms of self-assembly. This shows the importance of sample preparation and handling and the scope to achieve desired structures. It is interesting to note that the rather large globular substructures in the dendritic architectures of both proteins (see Figure 11) are similar despite the fundamentally different initial structures (fibrils vs.
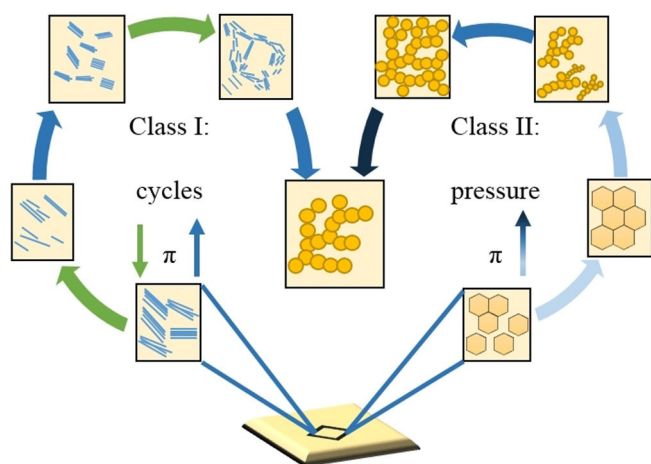
Figure 12. Schematic depiction of emergent dendritic structures. Left: Class I hydrophobin SC3 forms fibrils that persist during expansions (green arrows) and shorten over multiple cycles until dendritic superstructures emerge. Right: Class II HFBII forms closed membranes that transition into large dendritic aggregates at transfer pressures of 13 mN m^{-1} and above.

films). It seems that by reorganizing these two hydrophobins, particularly SC3, by multiple compression/release cycles at higher surface pressures and transfer to mica, one can find an underling similarity in their interaction patterns. We hope that this study may initiate further work towards a quantitative characterization of the structure formation under multiple mechanical constraints. Aside from a basic understanding of molecular processes during self-assembly, the control of their interfacial morphology on both a molecular and larger microscopic level is key to harnessing their potential in a plethora of applications.

Experimental Section

Protein Supply

SC3 was purchased from Sigma–Aldrich. The protein (1 mg) was dissolved in chilled trifluoroacetic acid (TFA). After removal of the liquid under a nitrogen stream, the sample was dissolved in water purified by using a Milli-Q system (Millipore) and samples (40 μg) were freeze-dried. N-terminal sixfold His-tagged HFBII was purchased from Biozol Diagnostica Vertrieb GmbH. The protein (1 mg) was dissolved in purified water, then samples (40 μg) were freeze-dried.

Pressure–Area Isotherms

The full isotherms were measured on a single-barrier Teflon trough of 4.71 and 22.43 cm^2 minimal and maximal area, respectively, equipped with an R&K controller and software (Riegler & Kirstein GmbH Potsdam, Germany). Purified water (Milli-Q) was used as a subphase for all measurements. The temperature was kept stable at $(20 \pm 0.5)\,°C$, and the compression speed was 2 Å(molecule min)$^{-1}$.

Samples of protein (40 μg) in chloroform (SC3) or water (HFBII) was spread onto the water surface and allowed to stabilize for 15 min (SC3) or 1.5 h (HFBII) before compression.

Langmuir–Schaefer Transfer and Atomic Force Microscopy

After compression to the desired surface pressure, the protein films were transferred to freshly cleaved mica that was rinsed with ethanol and briefly blow-dried with pressurized air directly before transfer by using a Filmlift FL-1 (MGW Lauda). Lifting occurred with an approach speed of 25 cm min^{-1}. After 24 s of contact with the interface, the substrate was lifted with a speed of 30 cm min^{-1}. The samples were dried in a desiccator for 48 h, then measured at RT by using a Multimode AFM (Veeco Metrology) equipped with Tapping Mode cantilevers (BudgetSensors) with a spring constant of 5 N m^{-1}, a nominal resonance frequency of 150 kHz, and a radius of < 10 nm.

Images were recorded by using NanoScope (v. 7.30, Veeco) software and processed by using Gwyddion 2.49 (freeware; http://gwyddion.net).

On average, three scans were recorded over the same area at a scanning rate of 0.5 Hz with a ratio of set-point amplitude to free amplitude of ≈ 0.8. Results are reproducible because similar structures were recorded over four different areas on average per sample. Height and phase images were recorded simultaneously.

Picture Editing and Determination of Height and Coverage

The AFM micrographs were plane leveled and fixed to zero. The surface coverages were determined. To optimize the calculations, the limit at which the protein was taken as a signal was 0.5 nm. Thus, anything above the muscovite surface plus a correction factor of 0.5 nm was used in calculation of the coverage.

The height distribution densities were calculated as noncumulative functions by using the Gwyddion software. A gauss 2 fit was used to determine the FWHM by using Equation (1)

$$f(x) = a_1 * \exp\left(-\left(\frac{(x - b_1)}{c_1}\right)^2\right) + a_2 * \exp\left(-\left(\frac{(x - b_2)}{c_2}\right)^2\right)$$

(1)

With parameters c_1 and c_2, the FWHM of the different maxima can be calculated according to Equation (2):

$$FWHM_i = 2 * \sqrt{2 * \ln(2)} * c_i / \sqrt{2}$$

(2)

Acknowledgements

Conflict of Interest

The authors declare no conflict of interest.

[1] J. G. H. Wessels, *Ann. Rev. Phytopath.* **1994**, *32*, 413–437.
[2] H. A. B. Wösten, M. L. de Vocht, *Biochimica et Biophysica Acta (BBA)—Reviews on Biomembranes.* **2000**, *1469*, 79–86.

[3] M. F. Gebbink, D. Claessen, B. Bouma, L. Dijkhuizen, H. A. Wosten, *Nat. Rev. Microbiol.* **2005**, *3*, 333–341.

[4] N. J. Talbot, M. J. Kershaw, G. E. Wakley, O. De Vries, J. Wessels, J. E. Hamer, *Plant Cell* **1996**, *8*, 985–999.

[5] X. Wang, F. Shi, H. A. B. Wösten, H. Hektor, B. Poolman, G. T. Robillard, *Biophys. J.* **2005**, *88*, 3434–3443.

[6] P. W. J. De Groot, P. J. Schaap, A. S. M. Sonnenberg, J. Visser, L. J. L. D. Van Griensven, *J. Mol. Biol.* **1996**, *257*, 1008–1018.

[7] D. J. Holder, N. O. Keyhani, *Appl. Environ. Microbiol.* **2005**, *71*, 5260–5266.

[8] H. A. B. Wösten, J. G. H. Wessels, *Mycoscience* **1997**, *38*, 363–374.

[9] V. Aimanianda, J. Bayry, S. Bozza, O. Kniemeyer, K. Perruccio, S. R. Elluru, C. Clavaud, S. Paris, A. A. Brakhage, S. V. Kaveri, L. Romani, J. P. Latge, *Nature* **2009**, *460*, 1117–1121.

[10] A. H. Kwan, R. D. Winefield, M. Sunde, J. M. Matthews, R. G. Haverkamp, M. D. Templeton, J. P. Mackay, *Proc Natl. Acad. Sc.i USA.* **2006**, *103*, 3621–3626.

[11] Q. Ren, A. H. Kwan, M. Sunde, *Biopolymers* **2013**, *100*, 601–612.

[12] L. Yu, B. Zhang, G. R. Szilvay, R. Sun, J. Jänis, Z. Wang, S. Feng, H. Xu, M. B. Linder, M. Qiao, *Microbiology* **2008**, *154*, 1677–1685.

[13] Y. Corvis, A. Walcarius, R. Rink, N. T. Mrabet, E. Rogalska, *Anal. Chem.* **2005**, *77*, 1622–1630.

[14] J. Hakanpää, A. Paananen, S. Askolin, T. Nakari-Setala, T. Parkkinen, M. Penttila, M. B. Linder, J. Rouvinen, *J. Biol. Chem.* **2004**, *279*, 534–539.

[15] A. Paananen, E. Vuorimaa, M. Torkkeli, M. Penttilä, M. Kauranen, O. Ikkala, H. Lemmetyinen, R. Serimaa, M. B. Linder, *Biochemistry* **2003**, *42*, 5253–5258.

[16] K. Kisko, M. Torkkeli, E. Vuorimaa, H. Lemmetyinen, O. H. Seeck, M. Linder, R. Serimaa, *Surf. Sci.* **2005**, *584*, 35–40.

[17] K. Kisko, G. R. Szilvay, E. Vuorimaa, H. Lemmetyinen, M. B. Linder, M. Torkkeli, R. Serimaa, *Langmuir* **2009**, *25*, 1612–1619.

[18] M. Sunde, A. H. Kwan, M. D. Templeton, R. E. Beever, J. P. Mackay, *Micron.* **2008**, *39*, 773–784.

[19] L. V. Govor, G. Reiter, G. H. Bauer, J. Parisi, *Appl. Phys. Lett.* **2006**, *89*, 133126-133126/3.

[20] O. Karthaus, T. Koito, M. Shimomura, *Mater. Sci. Eng. C* **1999**, *8–9*, 523–526.